Chemical Science

ROYAL SOCIETY OF CHEMISTRY

EDGE ARTICLE

View Article Online
View Journal | View Issue

Cite this: *Chem. Sci.*, 2021, **12**, 10871

All publication charges for this article have been paid for by the Royal Society of Chemistry

Control of dominant conduction orbitals by peripheral substituents in paddle-wheel diruthenium alkynyl molecular junctions†

Shiori Ogawa,[ab] Swarup Chattopadhyay,[c] Yuya Tanaka,[*ab] Tatsuhiko Ohto,[d] Tomofumi Tada,[e] Hirokazu Tada,[d] Shintaro Fujii,[f] Tomoaki Nishino[f] and Munetaka Akita[*ab]

Control of charge carriers that transport through the molecular junctions is essential for thermoelectric materials. In general, the charge carrier depends on the dominant conduction orbitals and is dominantly determined by the terminal anchor groups. The present study discloses the synthesis, physical properties in solution, and single-molecule conductance of paddle-wheel diruthenium complexes $\mathbf{1}^{R}$ having diarylformamidinato supporting ligands (DArF: *p*-R-C_6H_4-NCHN-C_6H_4-R-*p*) and two axial thioanisylethynyl conducting anchor groups, revealing unique substituent effects with respect to the conduction orbitals. The complexes $\mathbf{1}^{R}$ with a few different aryl substituents (R = OMe, H, Cl, and CF_3) were fully characterized by spectroscopic and crystallographic analyses. The single-molecule conductance determined by the scanning tunneling microscope break junction (STM-BJ) technique was in the 10^{-5} to 10^{-4} G_0 region, and the order of conductance was $\mathbf{1}^{OMe} > \mathbf{1}^{CF3} \gg \mathbf{1}^{H} \sim \mathbf{1}^{Cl}$, which was not consistent with the Hammett substituent constants σ of R. Cyclic voltammetry revealed the narrow HOMO–LUMO gaps of $\mathbf{1}^{R}$ originating from the diruthenium motif, as further supported by the DFT study. The DFT-NEGF analysis of this unique result revealed that the dominant conductance routes changed from HOMO conductance (for $\mathbf{1}^{OMe}$) to LUMO conductance (for $\mathbf{1}^{CF3}$). The drastic change in the conductance properties originates from the intrinsic narrow HOMO–LUMO gaps.

Received 30th April 2021
Accepted 1st July 2021

DOI: 10.1039/d1sc02407h

rsc.li/chemical-science

Introduction

Molecular junctions, which are composed of two electrodes with a bridging molecule, are fundamental nanostructures for molecule-based devices. Control of the charge carrier transport through the molecular junction, *i.e.* either an electron or a hole, is an essential requirement for thermoelectric materials, where both p- (hole transport) and n-type (electron transport) materials are necessary for a high performance series circuit.[1,2] Conduction orbitals close to the electrodes' Fermi energy levels determine the charge carrier and are mainly dominated by the terminal anchor groups, which connect to the electrodes.[3,4] The characteristics of the bridging linkers have a subtle effect with respect to the conduction of charge carriers because common organic molecules have a large separation between the HOMO and LUMO energies, which are far away from the Fermi energies of metal electrodes and, thus, structural modifications are often ineffective. As a rare example, Venkataraman and her coworkers have reported that the conductance pathway for dithiophene molecular wires with HOMO conducting thiomethyl anchor groups can be changed from the HOMO (hole) to the LUMO (electron) by insertion of tetra(thiophene-1,1-dioxide-2,5-diyls).[5] The oxidized thiophene part lowers the overall LUMO energy to change the dominant conduction orbitals, but it requires four repeating units. To date, however, control of the dominant conduction pathway *via* simple structural modifications, *i.e.* introduction of substituents, still remains elusive.

Chromium acetate ($Cr_2(OAc)_4$) synthesized in 1844 (ref. 6 and 7) and structurally characterized in 1951 was the first example of a dinuclear paddle-wheel metal complex (Fig. 1).[8] Since then, various kinds of paddle-wheel dimetal complexes

[a]*Laboratory for Chemistry and Life Science, Institute of Innovative Research, Tokyo Institute of Technology, 4259 Nagatsuta, Midori-ku, 226-8503, Yokohama, Japan. E-mail: ytanaka@res.titech.ac.jp; akitatit@icloud.com*

[b]*Department of Chemical Science and Engineering, School of Materials and Chemical Technology Tokyo Institute of Technology, 4259 Nagatsuta, Midori-ku, 226-8503, Yokohama, Japan*

[c]*Department of Chemistry, University of Kalyani, Nadia 741235, West Bengal, India*

[d]*Graduate School of Engineering Science, Osaka University, 1-3 Machikaneyama, Toyonaka, Osaka 560-8531, Japan*

[e]*Kyushu University Platform of Inter/Transdisciplinary Energy Research, Research Facilities for Co-Evolutional Social Systems, Kyushu University, 744 Motooka, Nishi-ku, Fukuoka 819-0395, Japan*

[f]*Department of Chemistry, School of Science, Tokyo Institute of Technology, 2-12-1 Ookayama, Meguro-ku, 152-8551, Tokyo, Japan*

† Electronic supplementary information (ESI) available: Synthesis, STM-BJ study, Vis-NIR absorption spectra, and DFT and TD-DFT studies. CCDC 2057135–2057137. For ESI and crystallographic data in CIF or other electronic format see DOI: 10.1039/d1sc02407h

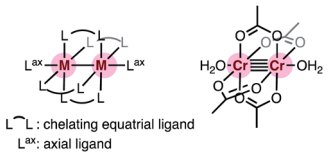

Fig. 1 Schematic representation of a paddle-wheel complex and the structure of chromium acetate with two axial water ligands.

have been studied extensively, especially by Cotton,[9,10] because they exhibit intriguing electrochemical, magnetic, and optical properties derived from the metal–metal interaction.[11,12] Recent advances in single-molecule conductance measurements using break-junction (BJ) methods allow scientists to unveil the conductance properties of inorganic paddle-wheel complexes.[13] For example, Chen and Peng reported that the conductance of the pentanuclear paddle-wheel complexes having the oligo-α-pyridylamine ligands and isothiocyanate anchor groups (Fig. 2a)[14] was dependent on the embedded metal atoms (M = Ni, Co, and Cr) as well as the metal–metal bond order. The single-molecule conductance of the linearly arranged undeca-nickel complex with the tetra-naphthyridyltriamide ligand was also determined (Fig. 2b).[15] On the other hand, carrier transport through the equatorial paddle-wheel ligands in the dimolybdenum complex was also reported recently (Fig. 2c).[16]

Organometallic paddle-wheel diruthenium complexes with two axial alkynyl ligands constitute an interesting class of molecules for materials science due to the narrow HOMO–LUMO gaps and the rich redox properties. The first example of this class of complexes, $Ru_2(ap)_4(C{\equiv}CPh)$, (ap = 2-anilinopyridinate), was reported by Cotton in 1986.[17] Later on, Ren *et al.* extensively explored their application in molecular devices.[18–22]

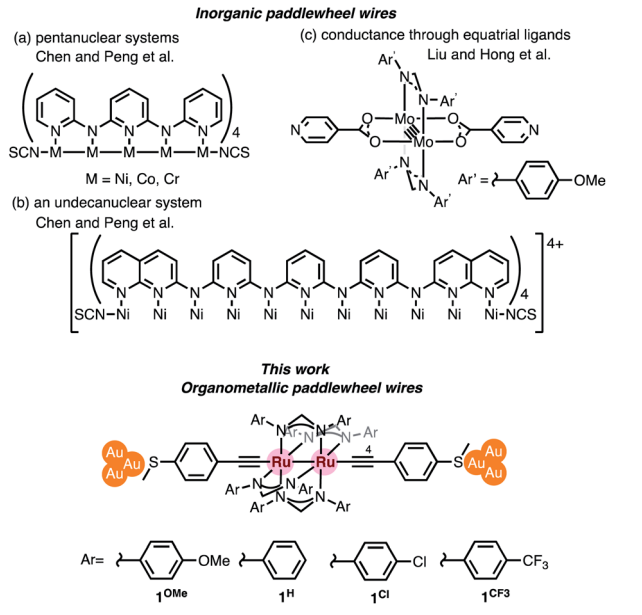

Fig. 2 Inorganic and organometallic molecular wires with paddle-wheel structural motifs.

To date, however, the single-molecule conductance measurement of organometallic paddle-wheel complexes remains to be studied. We describe, herein, the results of the single-molecule conductance study for a series of paddle-wheel diruthenium molecular wires $\mathbf{1^R}$ with diarylformamidinato supporting ligands (DArF*: p*-R-C_6H_4-NCHN-C_6H_4-R-*p*) and two axial thioanisylethynyl ligands (Fig. 2 bottom; R = OMe, H, Cl, and CF_3), in which the thiomethyl anchors show high affinity toward gold electrodes. The present study revealed a unique substituent effect of the aryl moieties in the supporting DArF ligands on the conductance, suggesting the dominant conduction band as well as the charge carrier conductance changed by the substituents.

Results and discussion

Synthesis and characterization

We prepared diruthenium dialkynyl complexes $\mathbf{1^R}$ (R = *p*-OMe, H, *p*-Cl, and *p*-CF_3) following the method previously reported by Ren *et al.*[23–25] Treatment of monochloro complexes $\mathbf{2^R}$ with an excess amount of lithiated 4-ethynylthioanisole afforded $\mathbf{1^R}$ in 17–49% yields. Conventional spectroscopic methods provide characteristic structural information of $\mathbf{1^R}$. The diruthenium dialkynyl complexes $\mathbf{1^R}$ are diamagnetic, and the single sets of ^{1}H NMR signals for the thioanisyl and DArF ligands indicate highly symmetrical structures of $\mathbf{1^R}$ in solution (Fig. S1a, S2a, S4a, and S5a†). HR-ESI-TOF-MS spectra of $\mathbf{1^R}$ contain molecular ion peaks corresponding to the deprotonated forms (Fig. S1e, S2f, S4h, and S5e†), and the ν(C≡C) vibrations appear in the range of 2092–2097 cm^{-1} (Fig. S1f, S2g, S4i, and S5f†). Purple crystals were grown by slow evaporation of mixed CH_2Cl_2/hexane solutions containing $\mathbf{1^H}$, $\mathbf{1^{Cl}}$, and $\mathbf{1^{CF3}}$. Molecular

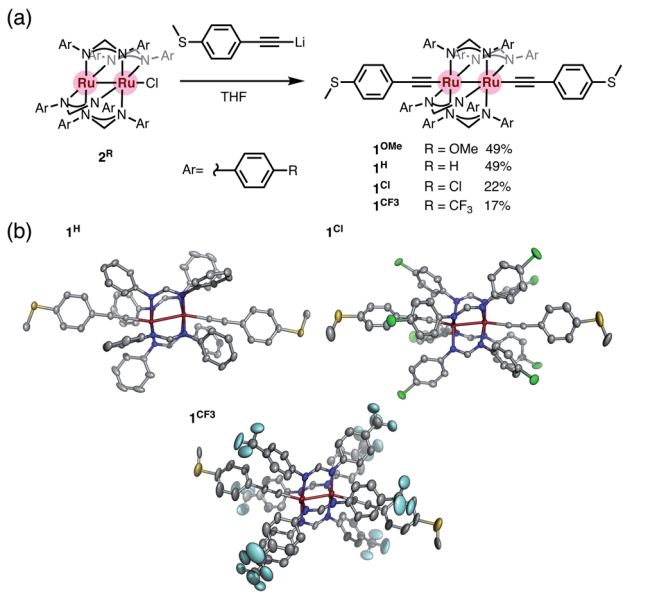

Fig. 3 (a) Synthesis of $\mathbf{1^R}$ (R = H, Cl, and CF_3). (b) Molecular structures of $\mathbf{1^H}$, $\mathbf{1^{Cl}}$, and $\mathbf{1^{CF3}}$ with thermal ellipsoids at the 50% probability level. Hydrogen atoms and disordered parts are omitted for clarity.

structures of $\mathbf{1}^{\mathbf{R}}$ (R = H, Cl, and CF_3)† shown in Fig. 3 are very similar to each other regardless of the substituents. The S···S distance is around 21 Å, and the Ru–Ru bond distance is *ca.* 2.55 Å ($\mathbf{1}^{\mathbf{H}}$; 2.5414(3) Å, $\mathbf{1}^{\mathbf{Cl}}$; 2.5468(3) Å, and $\mathbf{1}^{\mathbf{CF3}}$; 2.5521(7) Å), while short Ru–C≡ bond lengths (d_{Ru-C} = 1.97–1.99 Å) are observed. These structural features are typical for dialkynyl-$Ru_2(DArF)_4$ complexes with no net formal σ bond between the two Ru centers with the $\pi_4\delta_2\pi_4^*$ electronic configuration, where the electrons in the d_{z^2} orbitals are used for the Ru–C bonds.[26] The slightly bent Ru–Ru–C≡ linkages (154–166°) result from the second-order Jahn–Teller (SOJT) distortion (see below) to gain thermodynamic stability.[25,27,28]

STM-BJ study

We carried out single-molecule conductance measurements by the scanning tunneling microscope break-junction (STM-BJ) method.[29] In this method, a gold STM tip repeatedly moves in and out on a gold electrode, and the molecular junction accidentally forms during this process when molecules are present in the solution. The single process gives a long-conductance trace. A tetraglyme solution of $\mathbf{1}^{\mathbf{R}}$ (R = OMe, H, Cl, and CF_3, 0.25 mM) was soaked into the gold substrate and the break-junction measurements were performed using a gold STM-tip with 100 mV bias voltage. Individual traces show the steps in the 10^{-4} to 10^{-5} G_0 region (Fig. S6†). The 1D histogram constructed from 2000 successive traces reveals the peaks in the 10^{-4} to 10^{-5} G_0 region (Fig. 4). The 2D histogram of $\mathbf{1}^{\mathbf{H}}$ contains features extended up to ∼1.5 nm, which correspond to the molecular junction formation. Considering the snapback distance (∼0.5 nm),[30] the sum of the lengths well agrees with the S···S distance of $\mathbf{1}^{\mathbf{H}}$. On the other hand, the substituted analogues showed plateaus at shorter distances ($\mathbf{1}^{\mathbf{OMe}}$ and $\mathbf{1}^{\mathbf{Cl}}$: ∼1.3 nm and $\mathbf{1}^{\mathbf{CF3}}$: ∼0.6 nm) probably because the bulkier DArF ligands prevent the formation of molecular junctions and/or promote the breaking of molecular junctions. The single-molecule conductance was determined to be 3.4 (±1.0) × 10^{-4} G_0 ($\mathbf{1}^{\mathbf{OMe}}$), 5.7 (±0.7) × 10^{-5} G_0 ($\mathbf{1}^{\mathbf{H}}$), 5.6 (±1.7) × 10^{-5} G_0 ($\mathbf{1}^{\mathbf{Cl}}$), and 1.3 (±0.2) × 10^{-4} G_0 ($\mathbf{1}^{\mathbf{CF3}}$), with the trend of $\mathbf{1}^{\mathbf{OMe}} > \mathbf{1}^{\mathbf{CF3}} \gg \mathbf{1}^{\mathbf{H}} \sim \mathbf{1}^{\mathbf{Cl}}$. This trend is not in accord with the expectation that replacement with electron-withdrawing substituents (*cf.* σ: −0.27 (OMe), 0 (H), 0.23 (Cl), and 0.54 (CF_3)) deteriorates conductance because molecular wires with thioether anchor groups should prefer HOMO conductance caused by the energy alignment between the Au–sulfur lone pair bonds and the π-conjugated HOMO orbitals.[3,31]

Cyclic voltammetry and DFT study

To estimate the frontier orbital energies, we carried out electrochemical measurements of $\mathbf{1}^{\mathbf{R}}$ by cyclic voltammetry (Table 1, Fig. 5, [complex] = 1.0 mM in CH_2Cl_2, $[NBu_4][PF_6]$ = 0.1 M). The paddle-wheel complexes $\mathbf{1}^{\mathbf{R}}$ exhibit one 1e-oxidation and two successive 1e-reduction processes. The oxidation and reduction potentials cathodically shifted upon incorporation of the electron-withdrawing substituents ($E_{1/2}{}^1/E_{1/2}{}^2$; $\mathbf{1}^{\mathbf{OMe}}$: 0.12/−1.22, $\mathbf{1}^{\mathbf{H}}$: 0.19/−1.14, $\mathbf{1}^{\mathbf{Cl}}$: 0.38/−0.86, and $\mathbf{1}^{\mathbf{CF3}}$: 0.51/−0.65 V (*vs.* $FeCp_2/FeCp_2^+$)). The potential shifts for the reduction processes caused by substitution ($\Delta E_{1/2}{}^2 = E_{1/2}{}^{2\ \mathbf{1CF3}} - E_{1/2}{}^{2\ \mathbf{1H}} = 0.49$ V) are larger than those for the oxidation processes ($\Delta E_{1/2}{}^1 = E_{1/2}{}^{1\ \mathbf{1CF3}} - E_{1/2}{}^{1\ \mathbf{1H}} = 0.32$ V).

To obtain further insights into the electronic structures of molecular wires $\mathbf{1}^{\mathbf{R}}$, we performed density functional theory (DFT) calculations at the B3LYP/LanL2DZ,6-31G(d) levels combined with the CPCM continuum solvent method (CH_2Cl_2) (Table 1, Fig. 6 and S9†). The optimized structures well reproduce the X-ray structures with the $Ru_2(DPhF)_4$ core structures distorted from D_{4h} symmetry. The characteristics of the frontier

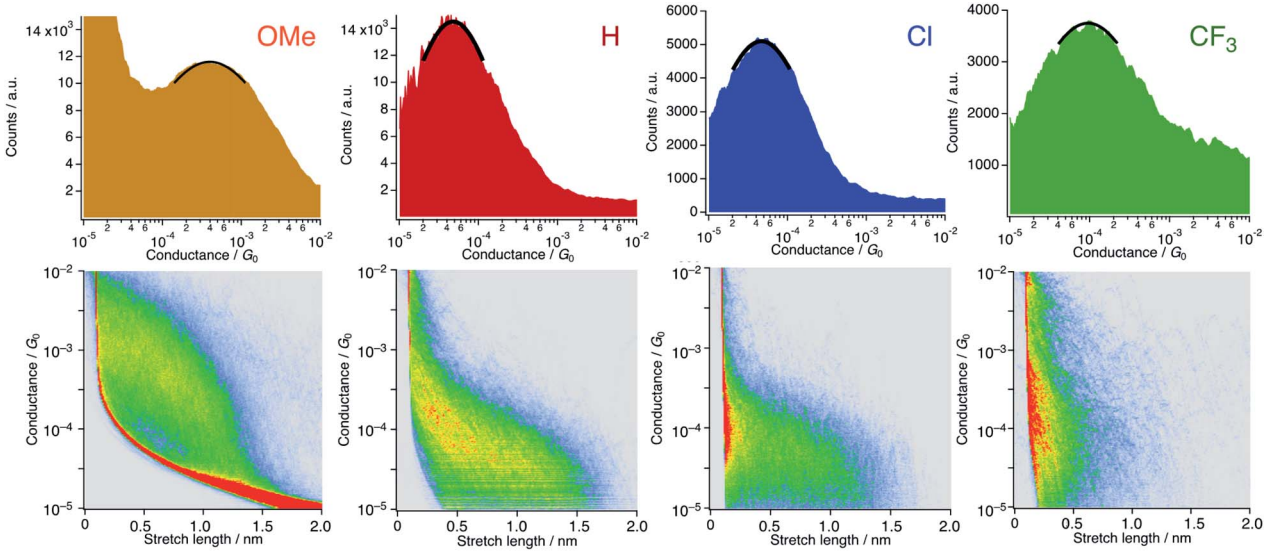

Fig. 4 1D and 2D histograms of $\mathbf{1}^{\mathbf{R}}$ (X = OMe, H, Cl, and CF_3) constructed from 2000 successive traces. [$\mathbf{1}^{\mathbf{R}}$] = 0.25 mM in tetraglyme. No data selection was performed.

Table 1 Summary of experimental and computational data for $\mathbf{1}^{R}$ (R = OMe, H, Cl, and CF_3)

Complex	$E_{1/2}^{1}$ [V]	$E_{1/2}^{2}$ [V]	$E_{1/2}^{3}$ [V]	$HOMO^{CV a}$ [eV]	$LUMO^{CV b}$ [eV]	Δ^{CV} [eV]	$HOMO^{DFT}$ [eV]	$LUMO^{DFT}$ [eV]	Δ^{DFT} [eV]	G_{exp} [10^{-5} G_0]	G_{calc} [10^{-5} G_0]	$HOMO^{NEGF}$ [eV]	$LUMO^{NEGF}$ [eV]	Δ^{NEGF} [eV]
$\mathbf{1}^{OMe}$	0.12	−1.22	−2.20	−5.22	−3.88	1.34	−4.92	−3.39	1.53	34 ± 10	165	−0.13	0.18	0.31
$\mathbf{1}^{H}$	0.19	−1.14	−2.11	−5.29	−3.96	1.33	−5.06	−3.60	1.46	5.7 ± 0.7	1.03	−0.15	0.12	0.27
$\mathbf{1}^{Cl}$	0.38	−0.86	−1.85	−5.48	−4.24	1.24	−5.19	−3.84	1.35	5.6 ± 1.7	5.33	−0.16	0.07	0.23
$\mathbf{1}^{CF3}$	0.51	−0.65	−1.66	−5.61	−4.46	1.15	−5.27	−4.00	1.27	13 ± 2.4	49.3	−0.10	0.04	0.14

[a] $HOMO^{CV}$ (in eV) = −($E_{1/2}^{1}$ (in V) + 5.1). [b] $LUMO^{CV}$ (in eV) = −($E_{1/2}^{2}$ (in V) + 5.1). [c] Calculated by the DFTNEGF study.

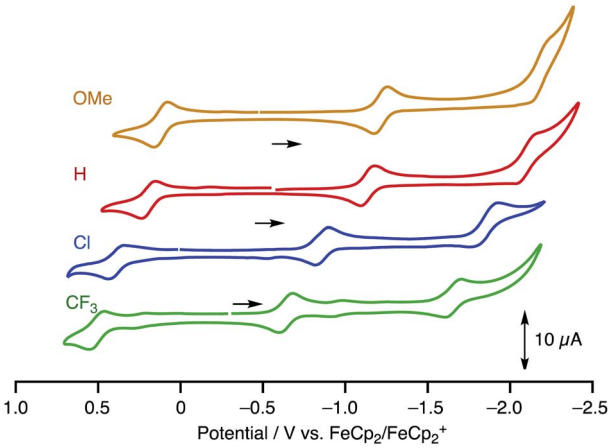

Fig. 5 CV charts of $\mathbf{1}^{R}$ (R = OMe, H, Cl and CF_3) ([complex] = 1.0 mM in CH_2Cl_2, $[NBu_4][PF_6]$ = 0.1 M, W.E. and C.E. Pt; R.E. Ag/Ag^+, at the scan rate of 100 mV s^{-1}).

orbitals of $\mathbf{1}^{R}$ are similar to each other. The highest occupied molecular orbitals (HOMOs), HOMO, HOMO–1 and HOMO–2, of $\mathbf{1}^{R}$ are extended over the $(Ru–C{\equiv}C–C_6H_4SMe)_2$ linkages with the anti-bonding ligand π* and ruthenium dπ* character, whereas the lowest unoccupied molecular orbitals (LUMOs) are localized on the Ru_2 δ* orbitals and the non-bonding N–C–N π orbitals of the DArF ligands. One notable feature of the HOMO and HOMO–1 is the overlap between the dπ* orbitals of the Ru cores due to the SOJT distortion as shown in Fig. 6.[32] As a result, the Ru_2 complexes gain some σ bonding nature between the two Ru atoms, which may enhance the hole transport process through the HOMO orbital.

The HOMO and LUMO energies ($HOMO^{DFT}/LUMO^{DFT}$) decrease from $\mathbf{1}^{OMe}$ (−4.92/−3.39 eV) to $\mathbf{1}^{H}$ (−5.06/−3.60 eV), $\mathbf{1}^{Cl}$ (−5.19/−3.84 eV) and then to $\mathbf{1}^{CF3}$ (−5.27/−4.00 eV), and the values are in good agreement with those obtained from the CV analysis ($HOMO^{CV}/LUMO^{CV}$). The LUMO energies are more sensitive to the substituents on the aryl substituents (R) in accord with the CV results probably due to a subtle contribution

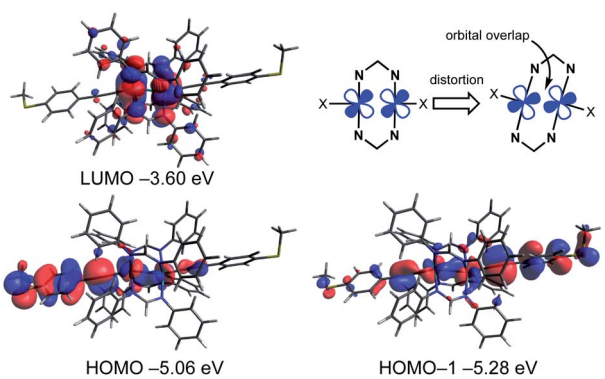

Fig. 6 Selected Kohn–Sham orbitals and their energies for $\mathbf{1}^{H}$ obtained by the DFT calculations (B3LYP/LanL2DZ,6-31G(d) and CPCM(CH_2Cl_2)) and the schematic representation of orbital overlap of Ru dπ* orbitals causing structural distortion.

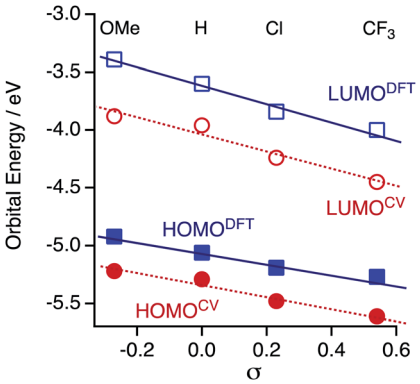

Fig. 7 Plots of the experimentally and theoretically obtained frontier orbital energies against the Hammett substituent constants σ.

of the aryl rings to the LUMO. As a result, the HOMO–LUMO gaps (Δ) decrease upon incorporation of the electron-withdrawing substituents (Δ^{DFT}; $\mathbf{1}^{OMe}$; 1.53, $\mathbf{1}^{H}$; 1.46, $\mathbf{1}^{Cl}$; 1.35, and $\mathbf{1}^{CF3}$; 1.27 eV). It is noted that the plots of the HOMO and LUMO energies estimated from the CV and DFT studies against the Hammett substituent constants σ show a good linear relationship (Fig. 7), as reported for the paddle-wheel dimolybdenum complexes with the DArF ligands.[33–35] Thus, the relationship between the molecule and electrode coupling should be considered to understand the unusual conductance trend by substituents.

DFT-NEGF study

To gain insights into the substituent effect of the paddle-wheel diruthenium molecular wires and the electronic structures of the molecular junctions, we carried out the DFT-non equilibrium Green's function (NEGF) calculations by using the TranSIESTA code[36] and the level-broadening approach developed by Tada *et al.*,[37] both of which gave similar results. Here, we discuss the results obtained from the TranSIESTA code for ***Au*-1^{R}-*Au*** (***Au***: gold electrodes).[38] The trend of the theoretically estimated conductance agreed well with that obtained from the break-junction study ($\mathbf{1}^{OMe} > \mathbf{1}^{CF3} \gg \mathbf{1}^{H} \sim \mathbf{1}^{Cl}$), showing the U-shaped plots (Table 1, Fig. 9a). The transmission spectra reveal many HOMO conduction orbitals within the range of 1.0 eV from the electrode's Fermi energy (E_F) in contrast to the lower number of the LUMO conduction orbitals. The conduction orbitals shown in Fig. 8b are altered by the substituents. The dominant transmission eigenchannels of ***Au*-1^{OMe}-*Au*** and ***Au*-1^{H}-*Au*** are akin to the HOMOs of $\mathbf{1}^{R}$ without the electrodes (Fig. 6), whereas LUMO-like δ^* orbitals appear for those of ***Au*-1^{Cl}-*Au*** and ***Au*-1^{CF3}-*Au***. Both the HOMO and LUMO conductance peaks (HOMO^{NEGF} and LUMO^{NEGF}) shift to the negative side upon replacement of the substituents on the DArF ligands with the electron-withdrawing ones (Fig. 8a and 9b).[39] For $\mathbf{1}^{OMe}$, the HOMO^{NEGF} (−0.13 eV) is closer to E_F than the LUMO^{NEGF} (0.18 eV), while the opposite trend is noted for $\mathbf{1}^{CF3}$ (HOMO^{NEGF}: −0.10 and LUMO^{NEGF}: 0.04). These results clearly indicate that the main conduction orbital changes from the HOMO (for $\mathbf{1}^{OMe}$) to the LUMO (for $\mathbf{1}^{CF3}$), leading to the conductance of $\mathbf{1}^{CF3}$ being

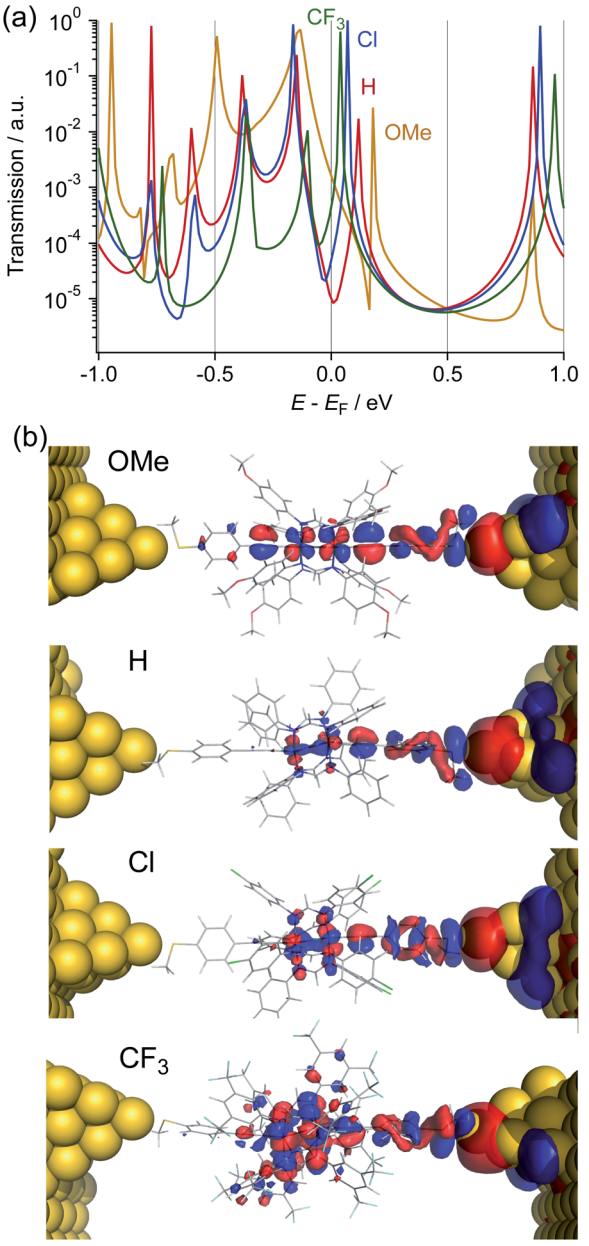

Fig. 8 (a) Transmission spectra and (b) the dominant transmission eigen channel at the Fermi level of ***Au*-1^{R}-*Au*** (R = OMe, H, Cl, and CF_3).

higher than that of $\mathbf{1}^{H}$ and $\mathbf{1}^{Cl}$. It is also noted that even the LUMO having the Ru_2 δ^* orbitals could be an efficient carrier transport pathway, though there is negligible contribution of the thioanisylethynyl ligands in $\mathbf{1}^{R}$. The effect of the substituents on the single-molecule conductance and transmission spectra reported so far was moderate or, sometimes, negligible because of their large HOMO–LUMO energy gaps.[40–42] The observed unique substituent effect should result from the fact that (1) the HOMO and LUMO conduction orbitals of $\mathbf{1}^{R}$ are located very close to E_F and, accordingly, the HOMO–LUMO gaps become very narrow, and (2) the LUMO energies being

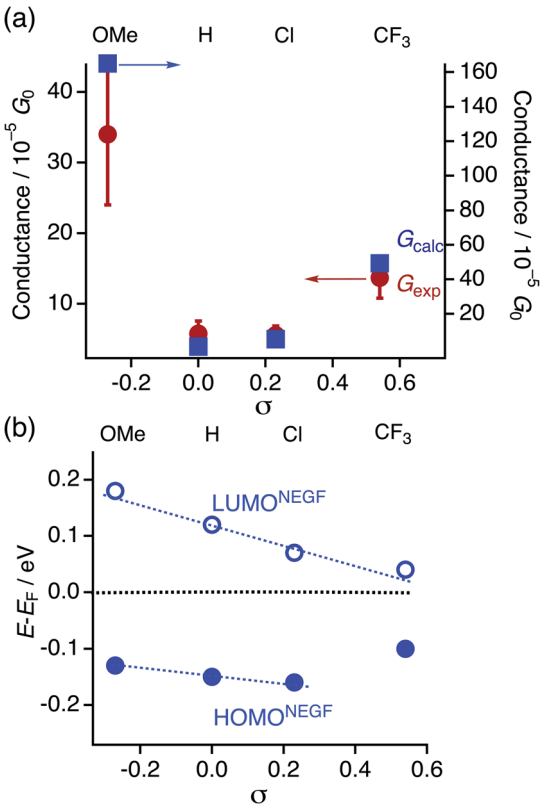

Fig. 9 Plots of (a) experimentally (G_{exp}) and theoretically obtained conductance (G_{calc}) and (b) the HOMO^{NEGF} and LUMO^{NEGF} against Hammett substituent constants σ.

more sensitive to the substituents causes the change of the conduction orbital from the HOMO to the LUMO.

Conclusion

We have reported the synthesis, electrochemical properties, and single-molecule conductance of paddle-wheel diruthenium complexes $\mathbf{1}^{\mathbf{R}}$ (R = OMe, H, Cl, and CF_3) having thioanisylethynyl axial ligands. The unique trend of the single-molecule conductance caused by the replacement of the substituents on the DArF ligands with electron-withdrawing ones results from the change of the dominant conduction orbital from the HOMO ($\mathbf{1}^{\mathbf{OMe}}$) to the LUMO ($\mathbf{1}^{\mathbf{CF3}}$) as revealed by the DFT-NEGF study. The drastic change of the conduction orbitals is caused by the narrow HOMO–LUMO gaps of the paddle-wheel diruthenium cores. Thus, the present study reveals the importance of molecular wires embedded with metal–metal bonds with narrow HOMO–LUMO gaps, which could facilely modulate conduction orbitals. Because the control of the conduction orbitals is vital for thermoelectric materials, paddle-wheel diruthenium complexes turn out to be fascinating platforms for these purposes.

Author contributions

SO, SC, YT, and MA conceived the project. SO, SC, and YT performed experiments. YT, TO, TT, and HT performed theoretical calculations. SF and TN discussed the STM-BJ results. YT wrote the first draft and MA critically reviewed and edited the manuscript. All authors commented on drafts, and approved the final manuscript.

Conflicts of interest

There are no conflicts to declare.

Acknowledgements

This work was supported by JSPS KAKENHI Grant Numbers 18K05139 and 21K05211. YT acknowledges research grants from the ENEOS Tonengeneral Research/Development Encouragement & Scholarship Foundation and the Asahi Glass Foundation. S. C acknowledges the Matsumae International Foundation Research Fellowship. The theoretical calculations were performed by using computers in the Research Center for Computational Science, Okazaki, Japan.

Notes and references

1 S. Park, H. Kang and H. J. Yoon, *J. Mater. Chem. A*, 2019, **7**, 14419–14446.
2 K. Wang, E. Meyhofer and P. Reddy, *Adv. Funct. Mater.*, 2020, **30**, 1904534.
3 T. A. Su, M. Neupane, M. L. Steigerwald, L. Venkataraman and C. Nuckolls, *Nat. Rev. Mater.*, 2016, **1**, 1–15.
4 M. Kiguchi and S. Kaneko, *Phys. Chem. Chem. Phys.*, 2013, **15**, 2253–2267.
5 E. J. Dell, B. Capozzi, J. Xia, L. Venkataraman and L. M. Campos, *Nat. Chem.*, 2015, **7**, 209–214.
6 E.-M. Peligot, *C. R. Acad. Sci.*, 1844, **19**, 609–618.
7 E.-M. Peligot, *Ann. Chim. Phys.*, 1844, **12**, 528–579.
8 J. N. Van Niekerk and F. R. L. Schoening, *Nature*, 1953, **171**, 36–37.
9 F. A. Cotton, *Acc. Chem. Res.*, 1969, **2**, 240–247.
10 F. A. Cotton, *Acc. Chem. Res.*, 1978, **11**, 225–232.
11 F. A. Cotton, C. Lin and C. A. Murillo, *Proc. Natl. Acad. Sci. U. S. A.*, 2002, **99**, 4810–4813.
12 I. P.-C. Liu, W.-Z. Wang and S.-M. Peng, *Chem. Commun.*, 2009, 4323–4331.
13 Y. Tanaka, M. Kiguchi and M. Akita, *Chem.–Eur. J.*, 2017, **23**, 4741–4749.
14 I.-W. P. Chen, M.-D. Fu, W.-H. Tseng, J.-Y. Yu, S.-H. Wu, C.-J. Ku, C. Chen and S.-M. Peng, *Angew. Chem., Int. Ed.*, 2006, **45**, 5814–5818.
15 P.-J. Chen, M. Sigrist, E.-C. Horng, G.-M. Lin, G.-H. Lee, C. Chen and S.-M. Peng, *Chem. Commun.*, 2017, **53**, 4673–4676.
16 M. Meng, Z. Tang, S. Mallick, M. H. Luo, Z. Tan, J. Liu, J. Shi, Y. Yang, C. Y. Liu and W. Hong, *Nanoscale*, 2020, **12**, 10320–10327.
17 P. A. Agaskar and F. A. Cotton, *Inorg. Chem.*, 1986, **25**, 15–19.
18 A. K. Mahapatro, J. Ying, T. Ren and D. B. Janes, *Nano Lett.*, 2008, **8**, 2131–2136.

19 H. Zhu, S. J. Pookpanratana, J. E. Bonevich, S. N. Natoli, C. A. Hacker, T. Ren, J. S. Suehle, C. A. Richter and Q. Li, *ACS Appl. Mater. Interfaces*, 2015, **7**, 27306–27313.
20 A. S. Blum, T. Ren, D. A. Parish, S. A. Trammell, M. H. Moore, J. G. Kushmerick, G.-L. Xu, J. R. Deschamps, S. K. Pollack and R. Shashidhar, *J. Am. Chem. Soc.*, 2005, **127**, 10010–10011.
21 J.-W. Ying, D. R. Sobransingh, G.-L. Xu, A. E. Kaifer and T. Ren, *Chem. Commun.*, 2005, 357–359.
22 S. Pookpanratana, I. Savchenko, S. N. Natoli, S. P. Cummings, L. J. Richter, J. W. F. Robertson, C. A. Richter, T. Ren and C. A. Hacker, *Langmuir*, 2014, **30**, 10280–10289.
23 T. A. Stephenson and G. Wilkinson, *J. Inorg. Nucl. Chem.*, 1966, **28**, 2285–2291.
24 C. Lin, T. Ren, E. J. Valente, J. D. Zubkowski and E. T. Smith, *Chem. Lett.*, 1997, **26**, 753–754.
25 C. Lin, T. Ren, E. J. Valente and J. D. Zubkowski, *J. Chem. Soc., Dalton Trans.*, 1998, 571–576.
26 F. A. Cotton and A. Yokochi, *Inorg. Chem.*, 1997, **36**, 567–570.
27 G. Xu, C. Campana and T. Ren, *Inorg. Chem.*, 2002, **41**, 3521–3527.
28 I. P.-C. Liu and T. Ren, *Inorg. Chem.*, 2009, **48**, 5608–5610.
29 B. Xu and N. J. Tao, *Science*, 2003, **301**, 1221–1223.
30 W. Hong, D. Z. Manrique, P. Moreno-García, M. Gulcur, A. Mishchenko, C. J. Lambert, M. R. Bryce and T. Wandlowski, *J. Am. Chem. Soc.*, 2012, **134**, 2292–2304.
31 P. Moreno-García, M. Gulcur, D. Z. Manrique, T. Pope, W. Hong, V. Kaliginedi, C. Huang, A. S. Batsanov, M. R. Bryce, C. Lambert and T. Wandlowski, *J. Am. Chem. Soc.*, 2013, **135**, 12228–12240.
32 A. Raghavan and T. Ren, *Organometallics*, 2019, **38**, 3888–3896.
33 C. Lin, J. D. Protasiewicz, E. T. Smith and T. Ren, *Inorg. Chem.*, 1996, **35**, 6422–6428.
34 T. Ren, *Coord. Chem. Rev.*, 1998, **175**, 43–58.
35 E. Van Caemelbecke, T. Phan, W. R. Osterloh and K. M. Kadish, *Coord. Chem. Rev.*, 2021, **434**, 213706.
36 M. Brandbyge, J.-L. Mozos, P. Ordejón, J. Taylor and K. Stokbro, *Phys. Rev. B*, 2002, **65**, 165401.
37 T. Tada, M. Kondo and K. Yoshizawa, *J. Chem. Phys.*, 2004, **121**, 8050–8057.
38 See the ESI.†
39 The HOMO energy of ***Au*-1^{CF3}-*Au*** showed a positive shift compared to those of the other substituents. This result is in accord with that of the level-broadening approach[37] (Fig. S13†).
40 L. Venkataraman, Y. S. Park, A. C. Whalley, C. Nuckolls, M. S. Hybertsen and M. L. Steigerwald, *Nano Lett.*, 2007, **7**, 502–506.
41 D. J. Mowbray, G. Jones and K. S. Thygesen, *J. Chem. Phys.*, 2008, **128**, 111103.
42 G. Yzambart, L. Rincón-García, A. A. Al-Jobory, A. K. Ismael, G. Rubio-Bollinger, C. J. Lambert, N. Agraït and M. R. Bryce, *J. Phys. Chem. C*, 2018, **122**, 27198–27204.